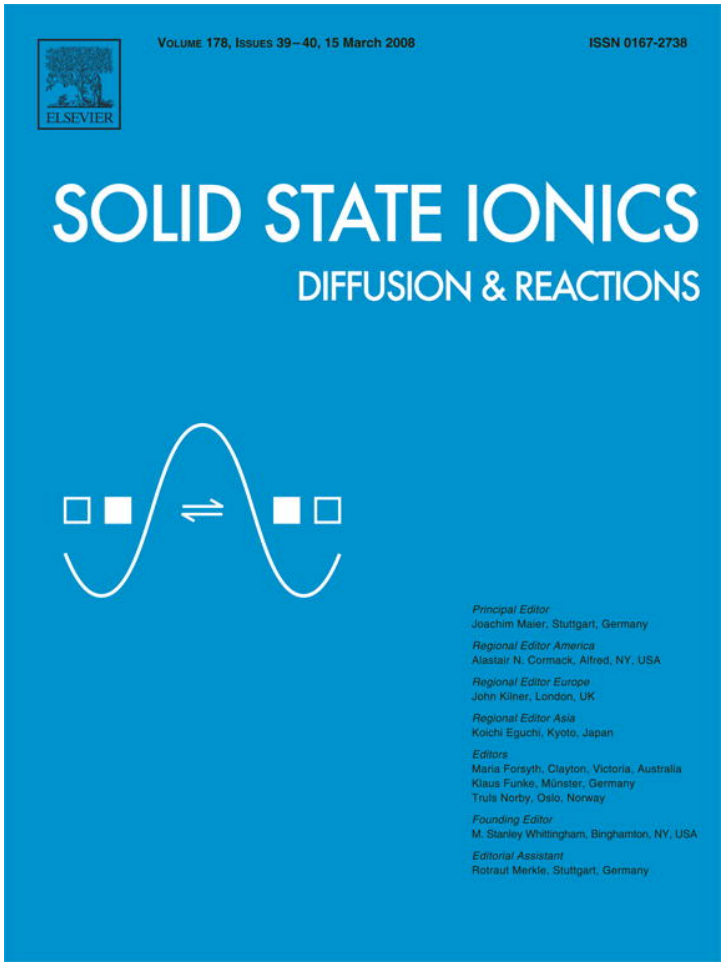

Available online at www.sciencedirect.com
ScienceDirect
Solid State Ionics 178 (2008) 1990–1997
SOLID STATE IONICS
www.elsevier.com/locate/ssi

Electrical characterization of dense and porous nanocrystalline Gd-doped ceria electrolytes

Seung Hwan Jo, P. Muralidharan, Do Kyung Kim *

Department of Materials Science and Engineering, Korea Advanced Institute of Science and Technology (KAIST), 373-1 Guseong-dong, Yuseong-gu, Daejeon 305-701, Republic of Korea

Received 27 July 2007; received in revised form 12 December 2007; accepted 25 December 2007

Abstract

The electrical properties correlated with microstructures of dense and porous three dimensional (3D) nanocrystalline $Ce_{0.9}Gd_{0.1}O_{1.95}$ (n-CGO) electrolytes prepared by the different sintering processes were investigated. The CGO pellets of dense-nano (DN-CGO), and porous-nano (PN-CGO) with grain size of 30~70 nm and their equivalent density pellets of dense coarse (DC-CGO) and porous coarse (PC-CGO) with larger grain size were prepared. The preparation of nanocrystalline CGO electrolytes with different grain sizes and densities was dependent on the different sintering processes, by controlled heating profiles, such as one step sintering and two steps sintering techniques. The electrical conductivity of CGO pellets was characterized using ac impedance spectroscopy (IS) as a function of temperature, oxygen partial pressure and grain size. The comparable electrical conductivity behavior for DN-CGO and DC-CGO may attribute to distant grain size level of DN-CGO from critical nano-grain size. On the other hand, a decreased electrical conductivity was observed in PN-CGO with grain size of 30 nm compared to its equivalent PC-CGO, including the porous conductivity correction, which confirms the existence of space charge region affecting the defect characteristics of nanocrystalline CGO. The electrical transport properties and microstructure parameters of the 3D nanostructured CGO electrolyte were discussed using the space charge model.

Keywords: CGO; Electrical conductivity; Nano-grain size; Two steps sintering; Solid oxide fuel cell; Space charge model

1. Introduction

In recent years, nanostructured ceramics have been extensively investigated due to the presence of a large fraction of grain boundaries that can lead to remarkable or enhanced electrical, magnetic, mechanical, optical, sensing, and biomedical properties compared with the microstructured materials. In particular, enhancement in the electrical transport properties in nanostructured solid electrolytes is a very important area for several applications, such as gas sensors, lithium ion batteries, intermediate temperature solid oxide fuel cells (IT-SOFCs), etc. [1–7]. In the literature, the electrical transport properties of oxides with grain size in the nanometric range have been mainly focused on thin film i.e., two dimensional (2D) with lesser consideration to the three dimensional (3D) nanostructured materials. The main reason for this is the difficulties encountered in the synthesis of fully-dense 3D nanocystalline ceramics with smaller nano-grain size (~30 nm) at normal sintering conditions, which lead to a faster grain growth and extinction of the nanostructure [8]. There have been few reports [9,10] on 2D nanostructures that demonstrate potential impact of high densities of grain boundaries (interfaces) in nanocrystalline solids consequently with enhanced ionic conductivity and defect formations for grain sizes approaching ~10 nm.

Among the novel solid electrolytes, ceria-based ceramics have been considered as the most promising electrolytes for IT-SOFCs because of their high ionic conductivity compared with yttria stabilized zirconia (YSZ) [11]. As a result, the researchers have focused their interest to investigate the nano-size effects of fully-dense 3D nanostructured Gd-doped CeO_2 (CGO) electrolyte. Chiang et al. [12], Tschope et al. [13], Kim et al. [14], Hwang et al. [15] have reported some important properties in 3D nanocrystalline

* Corresponding author. Tel.: +82 42 869 4118.
E-mail address: dkkim@kaist.ac.kr (D.K. Kim).

0167-2738/$ - see front matter © 2008 Elsevier B.V. All rights reserved.
doi:10.1016/j.ssi.2007.12.076

pure ceria such as the enhanced electronic conductivity, a reduced grain boundary impedance, and considerably smaller enthalpy of reduction compared to microcrystalline ceria. Kosacki et al. [16] have reported a remarkable enhancement in the total ionic conductivity in nanostructured CGO and YSZ thin films compared with the conductivity of large grain sized samples, whereas, conversely there were no reports to confirm the enhancement in the ionic conductivity for either 3D nanostructured stabilized zirconia or doped ceria. Therefore, the discrepancy of the enhanced ionic conductivity in thin film in comparison with 3D nanostructure may be related to spurious effects such as humidity or film substrate interactions in the case of the thin films [8]. There have been few comprehensible reports for heavily doped ceria that could reveal the nano-size effects on the electrical conductivity at critical grain size (~30 nm) [12,16].

The correlation between the microstructure parameters and electrical transport properties of conductive ceramics was described through many theoretical models such as the brick layer model proposed by Dijk et al. [17]. The brick layer model was described with 3D array of equal cubic grains and uniform grain boundary layers separating each other. Further, this model was modified into the space charge model by Maier et al. [18–20]. The distinguished feature of the space charge model was the consideration of charge distribution near the interface region, whereas, the simple neutral layer model considers only intrinsic defect concentrations and mobilities. Recently, Kim et al. [21] have reported the conduction mechanism for pure and slightly Gd doped ceria electrolytes based on the space charge model, in which the serial space charge zones perpendicular and parallel to ionic transport should be considered together to explain the conduction behaviors of nanocrystalline ionic conductors.

In the literature, there are several reports based on pressure-assisted routes for the synthesis of dense 3D nanostructured ceramics [22–25]. Alternatively, there is an advantageous controlled heating profile method to manipulate the microstructure during sintering process. For example, Chen et al. [26] have reported the synthesis of 3D fully-dense pure and doped yttria with grain size of 60 nm using a pressure less two steps sintering process. The suppression of the final-stage grain growth was achieved by exploiting the difference in kinetics between grain boundary diffusion and grain boundary migration. As a result, the two steps sintering process has recognized to be advantageous to synthesize fully-dense 3D nanostructured heavily doped ceria to study the effect of nano-size with the electrical transport properties.

In addition, there are some reports that describes the electrical properties of the nano-size grain porous ceramics synthesized by a partial sintering technique [15,27–30]. In particular, Mason et al. [15] have studied the electrical conductivity for the nano-size grain porous ceria ceramics using an impedance analysis. Also, Mason et al. [29] have reported the corrected electrical conductivity data considering the porosity conductivity of the zirconia doped ceria solid solution for a considerable comparison with data of the dense materials. In these porous ceramics, the pores were considered to be interconnected and followed the porosity correction based on Bruggeman symmetric medium theory [31]. Accordingly, it was described that biphasic materials have both high conductivity phase of the ceramics and low conductivity phase such as pores, cracks and second-phase inclusions, which were considered as microstructural defects in the porous ceramics.

In this paper, we have investigated the effect of nanostructure on the electrical transport characteristics of the Gd-doped ceria electrolytes. Nanostructured dense and porous pellets were prepared by a pressure less sintering process such as the one step sintering and the two steps sintering processes with controlled heating profiles. The correlation between the electrical properties and microstructure with various grain sizes and relative densities for the nano-size effects of CGO electrolytes was characterized using ac impedance spectroscopy as a function of temperature and oxygen partial pressure.

2. Experimental

Electrolyte ceramics were prepared from commercial 10 mole % Gd-doped ceria (CGO) ultrafine powder (99.9% pure, Nextech Materials, USA) with particle size of ~5 nm and specific area of 176.5 $m^2\ g^{-1}$. According to the Inductive Coupled Plasma (ICP) analysis, the most important impurities are: Si <20 ppm, Ca <20 ppm, K <100 ppm, Fe <35 ppm, Mg <53 ppm Al <41 ppm, Mn <2 ppm, Cr <15 ppm, Zn <3 ppm, Cu <3 ppm, Ti <1 ppm. Initially, to prepare dense and porous CGO nanostructures and their equivalent density samples with larger grain size, different sets of powder were calcined at 400 °C for 2 h and 900 °C for 10 h in air each separately and followed by ball-milling in isopropanol with zirconia media. After drying and granulation, the powders were uniaxially pressed and followed by CIP under 200 MPa. The dense-nano CGO (DN-CGO) pellet was prepared by the two steps sintering process. The powder compact was heated to 900 °C for 0 h with a heating ramp of 30 °C min^{-1} and cooled down to 870 °C and dwelled at that temperature for 10 h. The porous-nano CGO (PN-CGO) was prepared by a one step sintering process. The pellet was heat treated to minimum sintering temperature of 800 °C with a heating ramp of 5 °C min^{-1} and maintained for 30 min., which suppressed the grain growth and enabled to get the porous nanostructured CGO. The equivalent density pellets of dense-coarse CGO (DC-CGO) and porous-coarse (PC-CGO) were prepared by one step sintering at 1300 °C for 2 h and 1100 °C for 2 h with a heating ramp of 5 °C min^{-1}, respectively, using larger particle sized CGO powder that was calcined at 900 °C for 10 h.

To investigate the optimum parameters to produce dense CGO nanostructure via two steps sintering process, densification behavior of the DN-CGO pellet was investigated by a dilatometry (TMA92, SETARAM, Paris, France) in air at a constant heating rate of 30 °C min^{-1}. The grain sizes of the samples from each condition were characterized using a SEM (Philips XL30 FEG, Eindhoven, Netherland) for fractured surfaces of the pellets. The trace of impurity elements was detected through ICP analysis using ICP-AES (OPTIMA 4300DV, Perkin Elmer, Yokohama, Japan). The grain size distribution was estimated by the linear intercept method. The relative density of the samples at different sintering condition was measured by an Archimedes method.

For the impedance analysis, the surfaces of sintered pellets were polished and then gold electrode was sputtered onto either side of the pellets. The gold electrode coated pellet was

sandwiched between gold foils connected with platinum wires in a spring-loaded specimen holder. The electrical conductivity of the pellets was studied in the presence of air, O_2/N_2 mixtures, and CO/CO_2 mixtures for the various oxygen partial pressures by ac impedance spectroscopy using an Impedance/Gain-phase analyzer (Solartron 1260, Farnborough, UK) controlled by a computer program. The impedance spectra were measured over the frequency range 5 Hz to 10 MHz as a function of temperature from 250 to 500 °C and oxygen partial pressures of P_{O2} 10^{-33}–10^{-1} atm. The impedance data were collected ensuing correction using a standard nulling (open-circuit/short-circuit) procedure [32]. In the case of porous CGO pellets (PN-CGO and PC-CGO), the raw conductivity data were corrected considering the porosity conductivity for a meaningful comparison with the dense materials data. Accordingly, the electrical conductivity data for PN-CGO and PC-CGO were corrected on the basis of Bruggeman symmetric medium theory [31] using the Eq. (1):

$$\sigma_m = \sigma_h[(1-(3/2)f)] \text{ (when } \sigma_l = 0 \text{ negligible)} \quad (1)$$

where σ_m is the measured raw conductivity, σ_h is the conductivity of the high conducting phase and σ_l is the conductivity of the low conducting phase (pores), f is the volume fraction of the low conductivity phase (pores). The pore volume was calculated by the Archimedes method.

3. Results and discussion

3.1. Synthesis of 3D nanocrystalline CGO

The dense 3D nanocrystalline CGO pellet was prepared by the two steps sintering process. The shrinkage behavior of the CGO pellets during the two steps sintering process was monitored through dilatometric study and the results are presented in Fig. 1. Initially, the CGO pellet was heated to 900 °C at a heating rate of 30 °C min^{-1} to attain an intermediate density, then cooled down and dwelled at a lowered temperature for 10 h. Based on the literature report [26], the first step sintering temperature (T1: 900 °C) was determined to attain the intermediate density of ~75%. The second step sintering temperature was controlled below the first step temperature to obtain enhanced densification of the pellets while maintaining time was fixed to 10 h. During first step sintering temperature, attained relative densities of CGO pellets were 78.03% (Fig. 1a) and 77.54% (Fig. 1b). The sample attained a relative density of 85.65%, when the second step temperature was maintained at 850 °C for 10 h (Fig. 1a). However, the relative density increased to 92.95% as the second step temperature was raised to 870 °C (Fig. 1b). From these results, it can be concluded that the second step sintering temperature plays a critical role to determine the higher densification of the pellets. In addition, the difference between the first and the second step sintering temperatures should be smaller such that enhanced densification can be attained particularly for nanocrystalline CGO. The SEM fractographs for the two steps sintered CGO pellets are shown in Fig. 2. From Fig. 2a, it is observed the relative density estimated from Archimedes method was 76.58% and the grain size

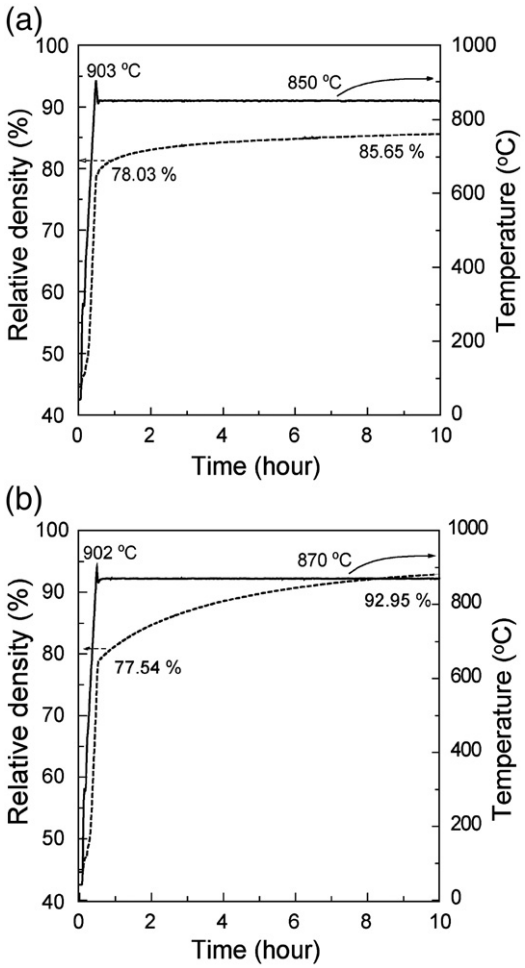

Fig. 1. The relative density and temperature as a function of time for the two steps sintering process of the CGO pellets, the second step temperature maintained at (a) 850 °C, (b) 870 °C.

estimated from the linear intercept method was 30 nm at first step sintering process. Fig. 2b and c show the SEM fractographs corresponding to the second step sintered pellets at 850 °C and 870 °C, respectively. From the microstructure analysis, it can be concluded that grain coarsening was occurred from 30 nm to 52 nm and to 72 nm after second step sintering for each condition. The density data obtained from Archimedes method were 86% (Fig. 2b) and 93% (Fig. 2c) for the second step sintered pellets at 850 °C and 870 °C, respectively and are agreed with those from shrinkage data as shown in Fig. 1. Fig. 3 presents the grain size vs. relative density plot for the one step and two steps sintered CGO pellets including the PN-CGO, DN-CGO, PC-CGO and DC-CGO. The open triangles denote one step sintered and the open circles correspond to the two steps sintered pellets. From Fig. 3, it is clearly observed that the two steps sintering process enables comparatively higher relative density than the one step sintering process, which is maintained with the similar grain size. It is comprehensible that the grain freezing effect was attained during the two steps sintering process. The obtained results indicated the similar grain freezing effect, but it was not in accordance with the ideal grain freezing behavior reported by I.-W. Chen [26]. Thus, the

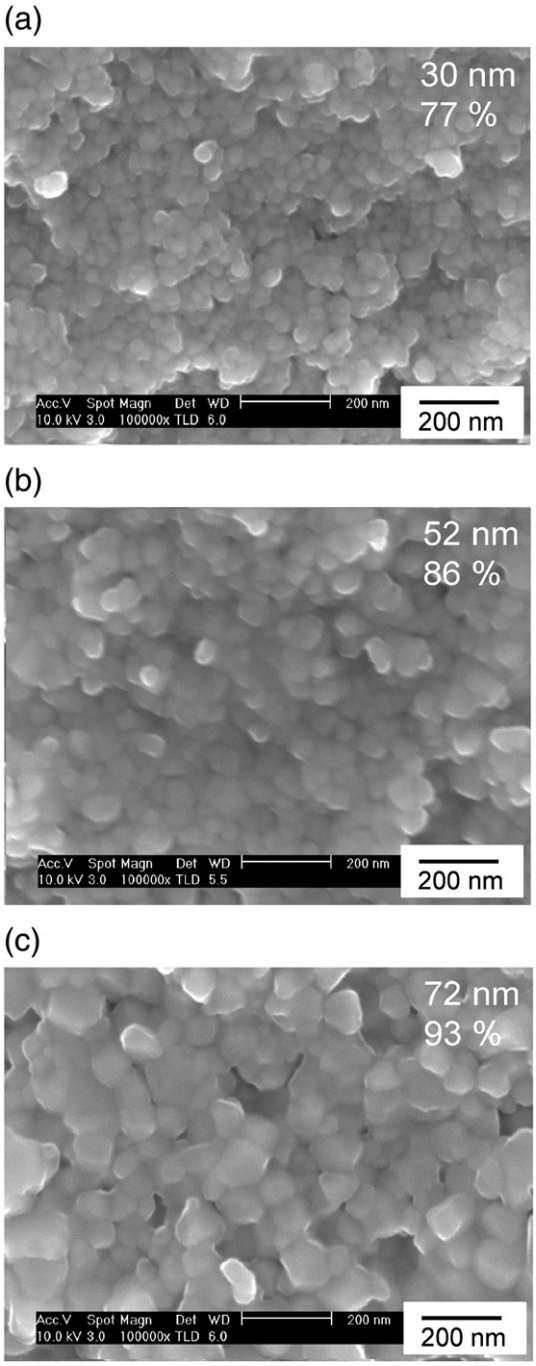

Fig. 2. The SEM fractographs for the CGO pellets prepared by the two steps sintering process (a) first step sintering (900 °C, 0 h), (b) second step sintering (850 °C, 10 h) and (c) second step sintering (870 °C, 10 h).

observed slight dissimilarity in grain freezing behavior may be due to green compact properties, which can be influence of the size, morphology and agglomeration of the particles.

3.2. Electrical properties of 3D nanocrystalline CGO

The electrical properties of the nanocrystalline CGO pellets prepared through the different sintering processes were characterized by ac impedance spectroscopy. The Table 1

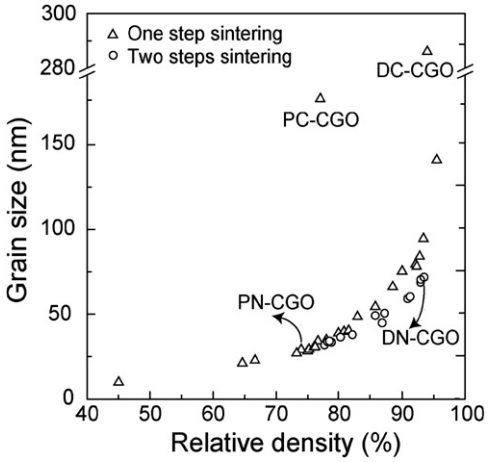

Fig. 3. Grain size as a function of relative density for the CGO pellets prepared by the one step and two steps sintering processes (open triangle: one step sintering, and open circle: two steps sintering).

represents the sample code, calcination temperature, sintering condition, grain size, relative density of the pellets used for the impedance measurement. The DN-CGO of 72 nm grain size with 93% of density was selected from the two steps sintered samples. To compare with the electrical conductivity behavior of DN-CGO pellet, the DC-CGO pellet (grain size of 286 nm, density of 94%) was synthesized by a one step sintering process using the CGO powder with large particle size to retain the equivalent density of DN-CGO. The PN-CGO pellet with the grain size of ~ 30 nm was prepared by one step sintering to illustrate the nano-size effects with the electrical conductivity at critical grain size. To compare the electrical conductivity and correlate the microstructure effect, the equivalent density PC-CGO pellet (grain size of 176 nm, density of 77%) was prepared with the coarsened CGO powder.

3.2.1. Dense nanocrystalline CGO

Fig. 4a and b show the complex impedance plots for the DN-CGO and DC-CGO pellets measured at 250 and 350 °C. It is evident to note the presence of three depressed semicircles within the measured frequency range. The first depressed semicircle at high frequency region corresponds to the bulk

Table 1
The sample code, calcination temperature, sintering condition, grain size, relative density

Sample[a] code	Calcination temp. (°C)	Sintering condition	Grain size (nm)	Relative density (%)
DN-CGO	400	Two steps sintering (900 °C, 0 h–870 °C, 10 h)	72	93
DC-CGO	900	One step sintering (1300 °C, 2 h)	286	94
PN-CGO	400	One step sintering (800 °C, 30 min)	30	74
PC-CGO	900	One step sintering (1100 °C, 2 h)	176	77

[a]DN denotes dense nanocrystalline, DC dense coarse, PN porous nanocrystalline, PC porous coarse, and CGO denotes Gd-doped ceria.

resistance and the second and the third depressed semicircles represent the grain boundary (core + space charge region) and the electrode resistances, respectively [33]. In Fig. 4a, the grain boundary depressed semicircle is slightly larger compared to bulk depressed semicircle, whereas these two components for DC-CGO have similar resistance. The calculated total electrical conductivity as a function of temperature is shown in Fig. 5 through Arrhenius plot. The total electrical conductivity of DN-CGO is slightly decreased compared to DC-CGO pellet and this decrease may be attributed to the higher resistance of grain boundary than that of the grain interior resistance. The calculated activation energy (E_a) from Arrhenius plot for DN-CGO is 0.65 eV, and that of DC-CGO is 0.62 eV. These values are well agreed with the reported data [34]. The temperature dependent electrical conductivity of DN-CGO and DC-CGO, which arises from the grain interior and grain boundary, was determined from ac impedance analysis as shown in Fig. 6. As estimated from Fig. 5, a slight decrease in the grain boundary conductivity was observed for DN-CGO in comparison with its equivalent density of DC-CGO (Fig. 6b), whereas the bulk conductivity remained same (Fig. 6a). These data supported the idea that the electrical conductivity of solid electrolyte can be controlled by microstructure changes. The slight decreased

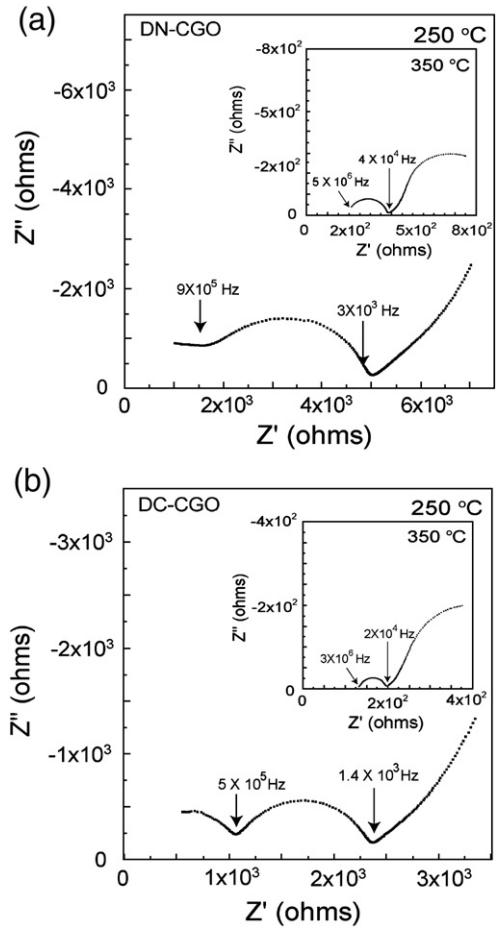

Fig. 4. Impedance spectra for (a) DN-CGO and (b) DC-CGO measured at 250 °C and inset at 350 °C.

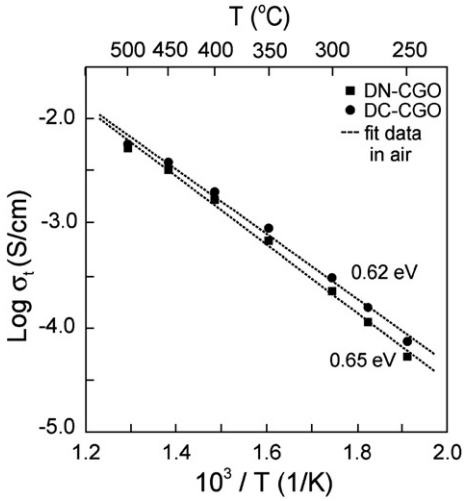

Fig. 5. Log σ_t versus 1000/T plots for the DN-CGO and DC-CGO pellets measured in air.

electrical conductivity for DN-CGO may be explained through the conventional brick layer model [17], without considering the nano-size effect, since the electrical conductivity behavior of DN-CGO is comparable to that of DC-CGO. Thus, the comparable electrical properties for DN-CGO and DC-CGO can be explained using this model based on considering the grain size above 70 nm, which is distant from the critical grain size. In the literature [35,36], similar phenomena were reported and explained using this model for microcrystalline solid electrolytes in which the grain size reduces result in the increase of the grain boundary resistance with increasing number of boundaries across the sample.

Important information regarding non-stoichiometry and the type of conduction can be obtained from the study of the electrical conductivity as a function of oxygen partial pressures. Fig. 7 shows the apparent ionic plateau at low oxygen partial pressures. This result implies that the general extrinsic conduction behavior of DN-CGO and DC-CGO is similar and independent of oxygen partial pressure range of 10^{-33}–10^{-1} atm within the temperature range of 400 to 500 °C. Thus, it can be concluded from the above results that DN-CGO has revealed comparable electrical properties with DC-CGO pellet. The comparable electrical properties for DN-CGO with micro-sized DC-CGO may be the nanostructure of DN-CGO is still distant from the critical grain size level to show distinguishable nano-grain size effects. The observed grain size above 70 nm with a high density was the limitation of the processing technique. As a result, it is essential to obtain critical nano-grain sized CGO pellets such that to elucidate the high interfacial density relationship with the electrical conductivity of the 3D nanocrystalline CGO samples.

3.2.2. Porous nanocrystalline CGO

Accordingly, PN-CGO with smaller grain size compared to DN-CGO was synthesized by a one step sintering process at 800 °C for 30 min. The complex impedance plots for the PN-CGO and PC-CGO pellets measured at 250 °C are shown in

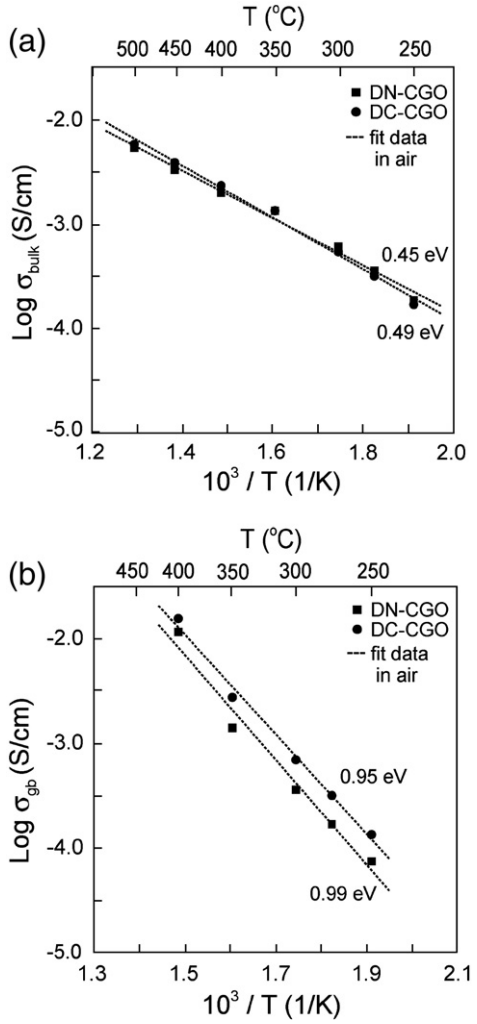

Fig. 6. Log σ versus 1000/T plots of (a) bulk (σ_b) and (b) grain boundary (σ_{gb}) conductivity for the DN-CGO and DC-CGO pellets measured in air.

Fig. 8a and b. It is clear to note the presence of two depressed semicircles (Fig. 8a) and the three depressed semicircles (Fig. 8b) within the limited frequency range. In the literature [30,37,38], it has been reported the microstructural defects such as cracks, pores and second-phase inclusions behave very similarly to the grain boundaries. Considering in the case of PN-CGO, the first depressed semicircle denotes the resistance of bulk, grain boundary and pores, and the second semicircle represents the electrode resistance. As suggested in brick-layer model calculation, in which grain interior and grain boundary semicircles may be virtually indistinguishable at the smaller grain sizes involved ceramics, same as PN-CGO in the present work [39]. The calculated total electrical conductivity as a function of temperature is represented as Arrhenius plots in Fig. 9. The raw conductivity data were corrected considering the volume fraction of porosity of the pellets based on Bruggeman symmetric medium theory using the Eq. (1) [29,31]. From Fig. 9, it is observed for the PN-CGO pellets a decreased total electrical conductivity and higher activation energy compared to those of PC-CGO as well as the dense CGO pellets (Fig. 5). Conversely, the total electrical conductivity including the porosity conductivity of PC-CGO shows a similar value with that of DC-CGO (Fig. 5). As a result, it can be concluded that the low conductivity of PN-CGO having the similar porosity of PC-CGO may be mostly attributed to the distinguished microstructural characteristic with high density of grain boundary area of the PN-CGO pellet and the porosity effects may be negligible. Therefore, the above results demonstrate that the possibility of ion blocking effects may be reasonably from the high density of grain boundaries in 3D nanocrystalline CGO electrolytes.

The distinguished electrical conductivity behavior in nanostructure can be interpreted by the space charge model which was proposed by Maier et al. [18–20]. In polycrystalline solid electrolytes, charged species, impurities and and/or defects, tend to segregate to grain boundaries in order to lower the strain and electrostatic energies of the system. The boundary charges are compensated by the formation of space charge in the adjoining grains. Thus, bulk ionic defects with like charge towards the boundary will be depleted while those with opposite charge will be accumulated in the space charge region. As a result, the accumulation or depletion of mobile charge carriers in the vicinity of interfaces imposes significant changes on the electrical conductivity of polycrystalline ionic conductors. Based on this model, if the bulk defect with high mobility is accumulated in the space

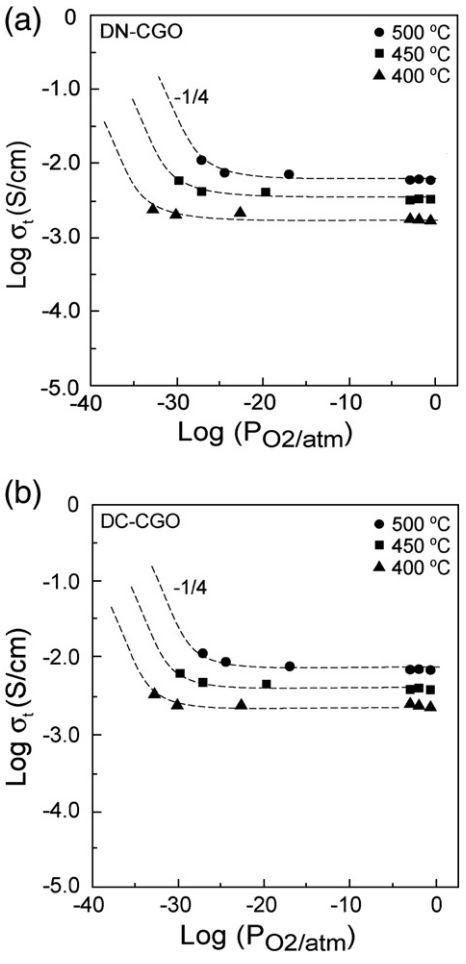

Fig. 7. Total electrical conductivity versus P_{O2} plots for (a) DN-CGO, (b) DC-CGO pellets measured at 400, 450 and 500 °C.

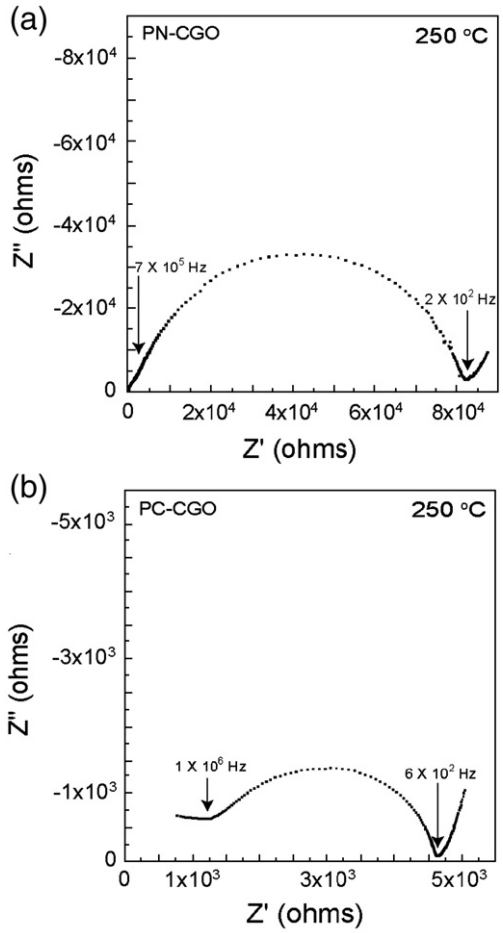

Fig. 8. Impedance spectra for (a) PN-CGO and (b) PC-CGO measured at 250 °C.

charge region, the overall electrical conductivity of the solid electrolyte should increase. However, in the case of most oxide ionic conductors, oxygen vacancy depleted space charge region is built up near grain boundary inside grain interior. This might decrease the grain boundary conductivity of solid electrolyte due

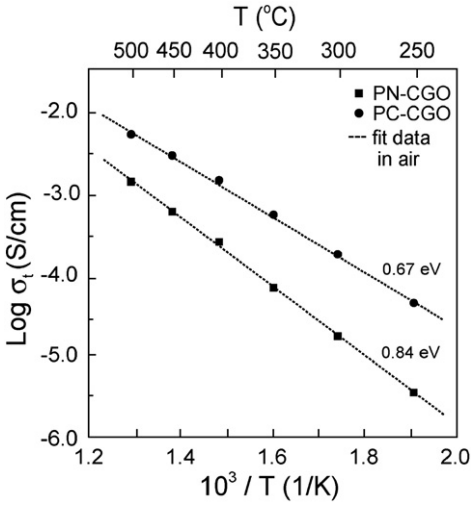

Fig. 9. Log σ_t versus 1000/T plots for the PN-CGO and PC-CGO pellets measured in air.

Table 2
The sample code, grain size, relative density and activation energy E_a calculated from total, bulk and grain boundary conductivity

Sample code	Grain size (nm)	Relative density (%)	Activation energy (eV)[a]		
			Total	Bulk	GB
DN-CGO	72	93	0.65	0.45	0.99
DC-CGO	286	94	0.62	0.49	0.95
PN-CGO	30	74	0.84		
PC-CGO	176	77	0.67		

[a] Calculated from Arrhenius plot.

to consecutive space charge zones perpendicular to ionic transport. These phenomena can be observed more prominently in the nanostructured oxides. Thus, this model well supports for the interpretation of results obtained for the nanostructured samples to explain the grain size dependence of thermopower and conductivity prediction [33,40,41]. In accordance with this model, the results imply that high density of the space charge zones perpendicular to the ionic transport may reduce significantly the ionic conductivity for PN-CGO pellet. As summarized in Table 2, it can be observed that the PC-CGO and DC-CGO pellets showed similar activation energy in spite of density variation while the PN-CGO pellet shows distinguishably high

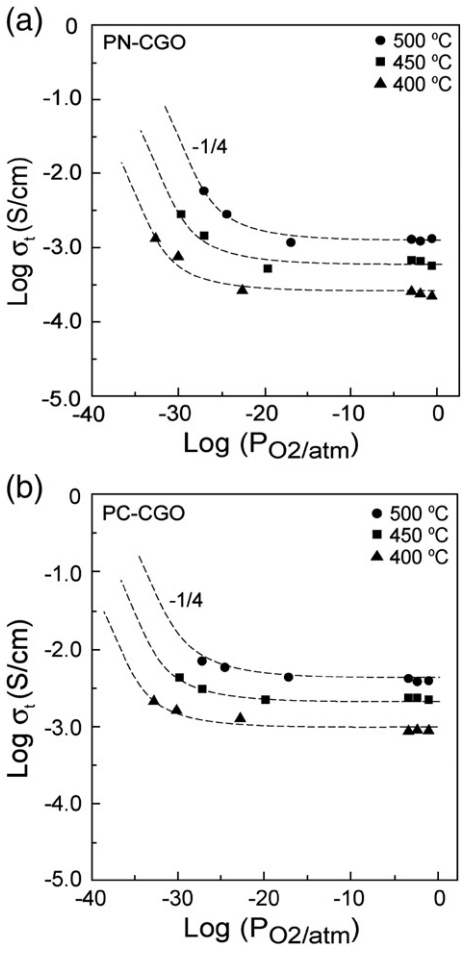

Fig. 10. Total electrical conductivity versus P_{O2} plots for (a) PN-CGO, (b) PC-CGO pellets measured at 400, 450 and 500 °C.

activation energy. This implies that the activation energy for electrical conduction was not significantly affected by density variation at coarse grain size level but dependent on grain size. Thus, the decreased electrical conductivity for PN-CGO may be attributed to the nano-grain size effects and negligible of the porous structure effects. The P_{O2} dependence of the electrical conductivity of PN-CGO was compared with PC-CGO, as shown in Fig. 10. In the case of PN-CGO, the observed electrical conductivity exhibited increasing behavior at low P_{O2} compared to that of PC-CGO. This behavior may be explained by enhanced electronic conductivity at low P_{O2} range due to relatively low reduction energy of Ce^{4+} to Ce^{3+} at nano-grain size of PN-CGO electrolyte compared to PC-CGO, in accordance with the reports in the literature [12,13].

4. Conclusion

The dense and porous 3D nanocrystalline CGO sintered pellets were successfully prepared by a one step and two steps sintering techniques. Electrical properties of DN-CGO and PN-CGO electrolytes and their equivalent density pellets were characterized by an impedance spectroscopy as function of temperatures and oxygen partial pressures. The observed electrical conductivity behavior for DN-CGO and DC-CGO was comparable as a result of the distant grain size level of DN-CGO from the critical nano-grain size. The decreased electrical conductivity and higher activation energy for electrical conduction were observed in nanocrystalline PN-CGO compared to microcrystalline PC-CGO, even with inclusion of the porosity conductivity. Considering space charge model, these may be attributed to the high grain boundary resistance caused by the serial space charge zones perpendicular to ionic transport in PN-CGO. Relatively, increasing behavior of electronic conductivity observed at lower P_{O2} in PN-CGO may be attributed to reduced activation energy of electron carrier generation at nano-grain size CGO. Thus, distinguished nano-size effect was correlated with electrical transport properties of the CGO electrolyte and explained using the space charge model.

Acknowledgments

This work was financially supported by the Core Technology Development Program for Fuel Cells of the Ministry of Commerce, Industry and Energy in Korea (Grant No. 10022724-2005-12) and the Korea Research Foundation Grant funded by the Korean Government (MOEHRD) (KRF-2005-005-J09701).

References

[1] H. Gleiter, Prog. Mater. Sci. 33 (1989) 223.
[2] D.D. Beck, R.W. Siegel, J. Mater. Res. 7 (1992) 2840.
[3] S. Sarat, N. Sammes, A. Smirnova, J. Power Sources 160 (2006) 892.
[4] T. Ishihara, J. Tabuchi, S. Ishikawa, J. Yan, M. Enoki, H. Matsumoto, Solid State Ionics 177 (2006) 1949.
[5] S.H. Park, H.I. Yoo, Solid State Ionics 176 (2005) 1485.
[6] J.H. Lee, S.M. Yoon, B.K. Kim, J. Kim, H.W. Lee, H.S. Song, Solid State Ionics 144 (2001) 175.
[7] S.H. Jo, J.H. Kim, D.K. Kim, Mater. Sci. Forum 539–543 (2007) 1373.
[8] H.L. Tuller, Solid State Ionics 131 (2000) 143.
[9] T. Suzuki, I. Kosacki, H.U. Anderson, Solid State Ionics 151 (2001) 111.
[10] N. Sata, K. Eberman, K. Eberl, J. Maier, Nature 408 (2000) 946.
[11] N.P. Brandon, S. Skinner, B.C.H. Steele, Ann. Rev. Mater. Res. 33 (2003) 183.
[12] Y.M. Chiang, E.B. Lavik, D.A. Blom, Nanostruct. Mater. 9 (1997) 633.
[13] A. Tschope, E. Sommer, R. Birringerm, Solid State Ionics 139 (2001) 255.
[14] S. Kim, J. Maier, J. Eur. Ceram. Soc. 24 (2004) 1919.
[15] J.H. Hwang, T.O. Mason, Z. Phys. Chem. 207 (1998) 21.
[16] I. Kosacki, H.U. Anderson, Y. Mizutani, K. Ukai, Solid State Ionics 152 (2002) 431.
[17] T.V. Dijk, A.J. Burgraaf, Phys. Status Solidi A 63 (1981) 159.
[18] J. Maier, Solid State Ionics 23 (1987) 59.
[19] J. Maier, Prog. Solid State Chem. 23 (1995) 171.
[20] S. Kim, J. Fleig, J. Maier, Phys. Chem. Chem. Phys. 5 (2003) 2268.
[21] S. Kim, J. Maier, J. Electrochem. Soc. 149 (2002) J73.
[22] U. Anselmi-Tamburini, J.E. Garay, Z.A. Munir, Scripta Mater. 54 (2006) 823.
[23] D.-J. Chert, M.J. Mayo, Nanostruct. Mater. 2 (1993) 469.
[24] J.R. Groza, Nanostruct. Mater. 12 (1999) 987.
[25] L. Gao, W. Li, H.Z. Wang, J.X. Zhou, Z.J. Chao, Q.Z. Zai, J. Eur. Ceram. Soc. 21 (2001) 135.
[26] I.-W. Chen, X.-H. Wang, Nature 404 (2000) 168.
[27] J.H. Hwang, T.O. Mason, M.F. Buehler, J.G. Darab, D.W. Matson, J.C. Linehan, Mater. Sci. Eng. A 204 (1995) 252.
[28] J. Lee, J.H. Hwang, J.J. Mashek, T.O. Mason, A.E. Miller, R.W. Siegel, J. Mater. Res. 10 (1995) 2295.
[29] M. Boaro, A. Trovarelli, J.H. Hwang, T.O. Mason, Solid State Ionics 147 (2002) 85.
[30] M. Kleitz, M.C. Steil, J. Eur. Ceram. Soc. 17 (1997) 819.
[31] D.S. Mclachlan, M. Blaszkiewicz, R.E. Newnham, J. Am. Ceram. Soc. 73 (1990) 2187.
[32] D.D. Edwards, J.H. Hwang, S.J. Ford, T.O. Mason, Solid State Ionics 99 (1997) 85.
[33] A. Tschope, S. Kilassonia, B. Zapp, R. Birringer, Solid State Ionics 149 (2002) 261.
[34] B.C.H. Steele, Solid State Ionics 129 (2000) 95.
[35] G.M. Christie, F.P.F. Van Berkel, Solid State Ionics 83 (1996) 17.
[36] R. Gerhardt, A.S. Nowick, J. Am. Ceram. Soc. 69 (1986) 641.
[37] M. Kleitz, L. Dessemond, M.C. Steil, Solid State Ionics 75 (1995) 107.
[38] L. Dessemond, R. Muccillo, M. Henault, M. Kleitz, Appl. Phys. A 57 (1993) 57.
[39] J.H. Hwang, D.S. McLachlan, T.O. Mason, J. Electroceram. 3 (1999) 7.
[40] A. Tschope, R. Birringer, J. Electroceram. 7 (2001) 169.
[41] J. Jamnik, J. Maier, S. Pejovnik, Solid State Ionics 75 (1995) 51.